Pure Appl. Chem., Vol. 78, No. 5, pp. 1025–1037, 2006.
doi:10.1351/pac200678051025

Structure and phase behavior of two-dimensional solids formed at interfaces*

Akira Inaba

Research Center for Molecular Thermodynamics, Graduate School of Science, Osaka University, Toyonaka, Osaka 560-0043, Japan

Abstract: Molecular monolayers adsorbed to solid surfaces such as graphite are distinct from the bulk in their physicochemical properties because of the 2D nature. In most cases, they form a well-defined 2D crystalline solid. We have been investigating such systems of various simple molecules by means of the synergetic use of X-ray diffraction, neutron scattering, and calorimetry. Selected examples illustrate that the reduced dimensionality has important consequences for the structure, dynamics, and phase behavior in the condensed state. In some cases, the similar solid monolayers are formed at the liquid–graphite interfaces, where they also show a rich variety of the structure and phase behavior. For the multicomponent system of those monolayers, mixing behavior is particularly interesting from both the structural and thermodynamic points of view. We also investigated ice crystallization from the solution, where a 2D nature was found in structure in the initial stage of crystallization.

Keywords: two-dimensional solids; interface; calorimetry; neutron scattering; X-ray diffraction; phase transitions.

INTRODUCTION

While molecular monolayers adsorbed to solid surfaces are both interesting and important in many aspects, the detailed structure and dynamics as well as the phase behavior are difficult to investigate. Such investigations require probes that are sensitive enough to study the tiny quantities of material present in the adsorbed layers without being dominated by the much larger quantities of bulk materials. In a few decades, however, exfoliated graphite has become popular in adsorption studies as one of the most appropriate substrates to meet conflicting requirements: large surface area (typically 10–50 $m^2\ g^{-1}$) and small extent of surface heterogeneity. The former makes it easy to apply several powerful methods of solid-state science, and the latter allows us to distinguish properties intrinsic to adsorption on perfect substrates from those due to substrate heterogeneity. In addition, the graphite basal planes can be made to adopt a preferred orientation, providing a means to probe the adsorption structure and dynamics parallel and perpendicular to the surface separately. The results thus obtained, therefore, can stand theoretical analysis.

The monolayers physically adsorbed on graphite are certainly the approach to 2D arrangements of molecules [1]. There is a competition between the various types of intermolecular and admolecule–substrate interactions, resulting in a rich variety of 2D structures. Even in the triangular structures for the monolayers of small molecules, the 2D crystalline phases can be commensurate or incommen-

*Paper presented at the 40th IUPAC Congress, Beijing, China, 14–19 August 2005. Other presentations are published in this issue, pp. 889–1090.

surate with respect to the substrate lattice. Phase transitions within the layers may involve not only the in-plane azimuthal orientations of the molecules, but also the out-of-plane tilts, including the extreme case of a change from horizontal to perpendicular. When multicomponents are involved in the monolayer formation, the mixing behavior is also interesting.

The experimental methods that we have employed are calorimetry, X-ray diffraction, and neutron scattering. The first is powerful in detecting phase transitions and characterizing the phase behavior. X-ray diffraction is still applicable to investigate the structure of 2D solids. The role of neutron techniques is unique, although they are not generally surface-specific: Neutrons can probe the structure and dynamics of a single component of an adsorbed layer that is only a single molecule thick even in the presence of a much larger excess of bulk phases.

In this article, we are mostly concerned with the submonolayer of rather simple molecules physically adsorbed on graphite. Several examples are illustrated to show how the reduced dimensionality alters the structure and phase behavior. In addition, we found that in some cases the similar 2D solids are formed at the liquid–graphite interfaces. Some of the examples are also described. Finally, the 2D nature of the ice obtained from the solution is presented.

DIPOLAR ORDERING IN CO MONOLAYER ON GRAPHITE

Nitrogen and carbon monoxide are very similar in physicochemical properties because of the similarity of molecular properties except for the polarity. The CO exhibits residual entropy down to absolute zero in the bulk matter [2], whereas N_2 is completely ordered. Because of the small dipole moment, the occurrence of a random head–tail disorder was suspected in its low-temperature phase (α-CO). A careful reexamination [3] found a small anomaly in heat capacity around 18 K and detected appreciable enthalpy relaxation, which was interpreted as due to a glass transition which arises from freezing-out of molecular end-for-end reorientation. The residual entropy has thus been understood as a kinetic effect.

With respect to the monolayers adsorbed on the surface of graphite, both N_2 and CO molecules are in registry with the underlying hexagons: The centers of mass assume the well-known $(\sqrt{3} \times \sqrt{3})R30°$ commensurate structure [4] with the nearest-neighbor separation of 0.426 nm, which is much longer than that in the bulk solids (0.399 nm). Because of the low dimensionality and larger intermolecular separation, the thermodynamic behavior was supposed to be changed dramatically from those of the bulk. The measured molar heat capacities of the monolayers of N_2 and CO on graphite are plotted in Fig. 1a [5]. While no anomaly was observed for N_2/graphite below 15 K, a peak in heat capacity was found at 5.4 K for CO/graphite. The molar entropies were calculated by integrating C/T and are illustrated in Fig. 1b, where the heat capacity below 3 K was assumed to be represented by $C \propto T^2$. The difference in the magnitude of molar entropy between N_2 and CO at 14 K amounts to 6.08 J K^{-1} mol^{-1} which is fairly close to R ln 2 (= 5.76 J K^{-1} mol^{-1}). This is in contrast to the case of the bulk. A justification of the realization of the completely ordered phase at the lowest temperature was made with the aid of the third law of thermodynamics [6], in this case, from the comparison of the molar entropy derived from the measurements of heat capacity and that from the enthalpy of adsorption. A complete analysis [7] showed that those two molar entropies agreed well for both N_2 and CO monolayers. Despite the effort to determine the ordered structure of CO/graphite by neutron diffraction [8], however, the head–tail arrangement is still not known for certain.

The situation is quite analogous in N_2O, which also has an appreciable quadrupole moment, a very small dipole moment, and the same structure in both the bulk state and adsorbed monolayer. In contrast to the case of CO/graphite, however, no anomaly was observed in heat capacity down to 3 K for the solid monolayer N_2O/graphite [9], suggesting that the N_2O molecules are orientationally ordered and the disorder of molecular head–tail orientation has become frozen. Of major importance is the fact that the magnitude of the activation energy for 180° flips is very sensitive to the intermolecular separation as well as the magnitude of quadrupole and dipole moments and the size of molecule. Such a subtle effect might push the balance either way.

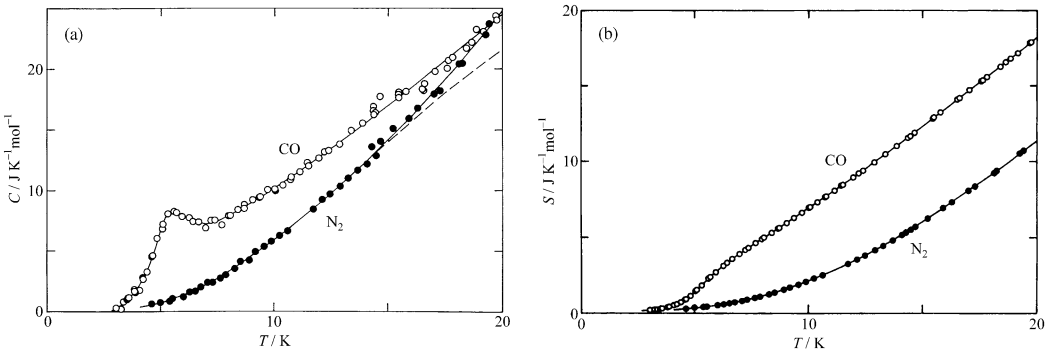

Fig. 1 (a) Heat capacities of the monolayers of N_2 and CO on graphite. For N_2/graphite, the normal heat capacity is illustrated [5]. (b) Entropies of the monolayers of N_2 and CO on graphite [5].

ROTATIONAL TUNNELING IN METHANE MONOLAYERS ON GRAPHITE

Methane also adopts the $(\sqrt{3} \times \sqrt{3})$ $R30°$ commensurate structure at coverages well below a monolayer: The molecules sit on the graphite surface in such a way that every third of the graphite structure is occupied by a methane molecule, where every molecule senses a trigonal field. Here, it is interesting to note that this deduction was not derived from any structural determination, but from the rotational dynamics of methane molecules [10]. Rotational tunneling occurs when the wave functions of two or more identical atoms with degenerate librational energy levels overlap. The energy levels split in order to lift the degeneracy. This splitting is referred to as tunneling and is observable at low temperatures when the effect of thermal vibrations is small. It is a particularly sensitive probe of the interatomic forces responsible for the rotational potential in the materials. The neutron-scattering technique has held a central position in such studies, since the tunneling spectrum can be observed directly.

The rotational tunneling spectra of CH_4/graphite were first analyzed in [10]. In a tetrahedral potential, there are three librational energy levels, A, T, and E, but in the trigonal field of the surface and surrounding molecules the degeneracy of the T level is split to give a total of four levels. Five transitions occur in the incoherent neutron-scattering spectra, all of which were observed. The spectra were quantitatively explained in terms of just two parameters, which are related to the heights of the barriers to rotation about the unique C–H bond normal to the surface and about one of the three equivalent C–H bonds pointing toward the surface. A later experiment with higher resolution [11] revealed extra detail in the spectra (Fig. 2). An extra parameter was introduced, representing the interaction between orientations connected by two-fold rotation to explain the data adequately.

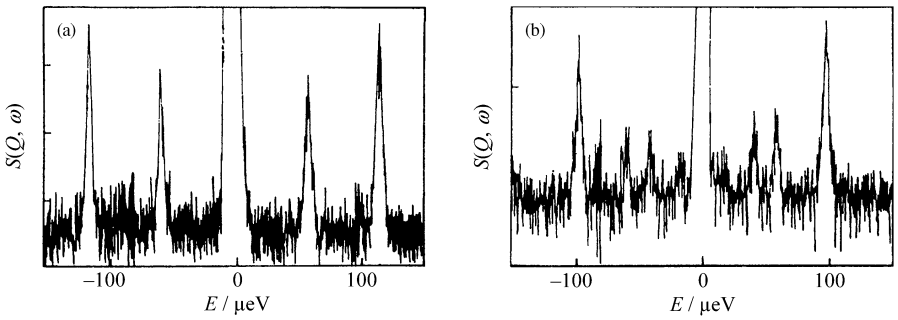

Fig. 2 Rotational tunneling spectra of CH_4/graphite obtained at 4.5 K [11]. (a) $Q_{\perp}$, (b) $Q_{||}$.

We also examined the conversion between the different spin species. With trace amounts of oxygen, the spectra at 0.35 K (Fig. 3a) clearly showed that the spin system does come to equilibrium [12], where the rate of spin conversion depends on the temperature and the amount of oxygen [13]. The equilibrium heat capacity of the whole system including the spin system was obtained (Fig. 3b). Without oxygen, on the other hand, the spectra revealed that the spin system is not in equilibrium with the lattice. The heat capacity measurement [13] indicated that the spin conversion between T and E would still be rapid in the pure CH_4/graphite (Fig. 3b), which is totally different from the bulk case.

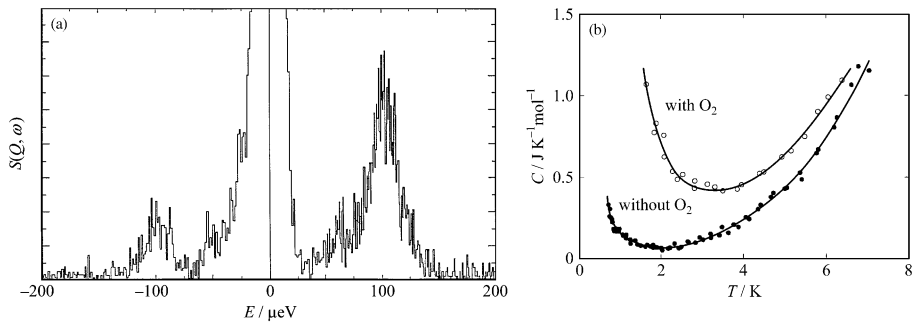

Fig. 3 (a) Rotational tunneling spectrum obtained at 0.35 K for CH_4/graphite with 1 % of O_2, $Q_{||}$ [12]. (b) Heat capacities of CH_4/graphite with and without O_2 [13].

The partial deuteration of CH_4 is intriguing since it defines a molecular axis: When the molecules interact with sites of lower symmetry, a distinction can be made between orientational levels, where the splitting stems from the change of the molecular axis relative to the site symmetry axes, and tunneling levels, where the splitting arises from overlap between equivalent molecular orientations. The neutron-scattering and heat capacity measurements sample the manifolds of energy states in different ways. High-resolution neutron spectra for CH_3D/graphite (Fig. 4) made it possible to give an unambiguous assignment of the tunneling spectra [11], which is different from that previously proposed [14]. Heat capacity measurements suggested that the spin conversion is much faster in CH_3D/graphite [15] and showed a Schottky anomaly (Fig. 5a) resulting from the difference in energy between states with the single deuterium atom pointing away from the surface (D-up) and states where the deuterium atom is part of the tripod of atoms pointing toward the surface (D-down). The energy difference is 380 μeV with the D-down configuration being the more stable. The combination study determined the whole energy scheme (Fig. 5b) [16], which significantly refined the understanding of orientational and tunneling behavior over what was obtainable from one type of data alone.

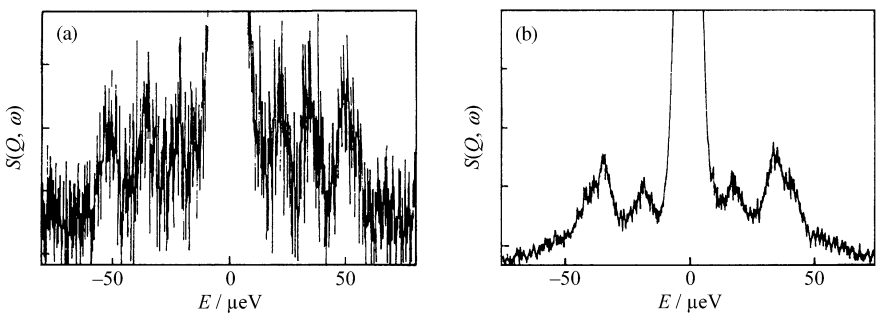

Fig. 4 Rotational tunneling spectra of CH_3D/graphite obtained at 4.5 K [11]. (a) $Q_{\perp}$, (b) $Q_{||}$.

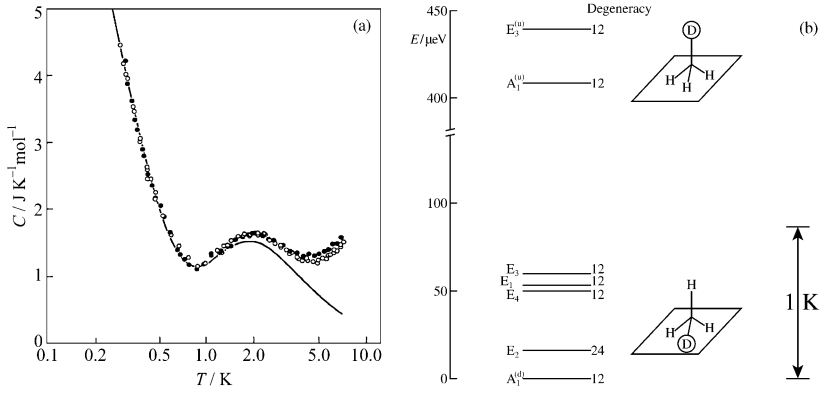

Fig. 5 (a) Heat capacities of CH_3D/graphite at two different coverages. The solid curve is calculated from the energy scheme. The discrepancy between them comes from the 2D lattice vibrations [16]. (b) Energy scheme for CH_3D/graphite [16].

PHASE TRANSITIONS IN CH_3F AND CH_3Cl MONOLAYERS ON GRAPHITE

The interest in the methyl halide (CH_3X) series adsorbed on graphite is that a varying balance of three factors would determine the structure of the monolayer; the large dipole moments, the interaction of the halogen atom with the surface, and the nonbonding interaction between halogen atoms. Unexpected phase transitions were observed in the CH_3F and CH_3Cl monolayers.

Neutron diffraction and heat capacity measurements were combined to study the structure and phase transitions occurring in CH_3F/graphite (Fig. 6) [17]. There is a sharp anomaly in heat capacity, corresponding to melting at 124 K, and a small anomaly around 100 K. Neutron diffraction of CD_3F/graphite at 80 and 105 K found three and two Bragg peaks, respectively [17], indicating that both 2D phases are ordered being commensurate with the underlying substrate ($3 \times \sqrt{3}$). The small transition entropy is thus understandable because of the order–order type.

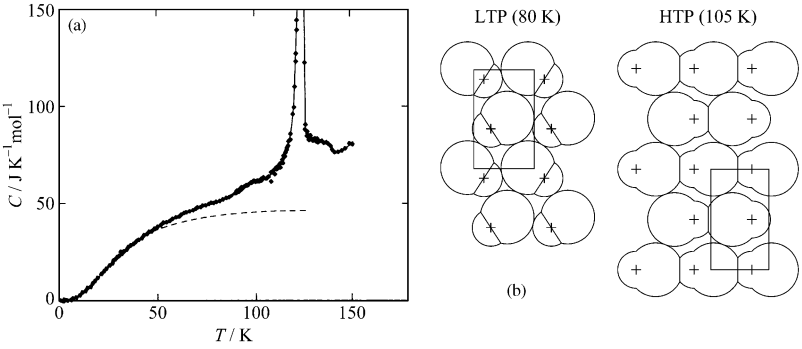

Fig. 6 (a) Heat capacity of CH_3F/graphite [17]. (b) Structure of the low- and high-temperature phases of CD_3F/graphite [17].

For CH_3Cl/graphite, two different 2D solid phases exist depending on the coverage [18–20]. The low-density phase (ca. 5 molecules nm^{-2}) melts at 120 K, whereas the high-density phase (ca. 7 molecules nm^{-2}) melts at 146 K. There is a coexistence region in between, where the melting point becomes lower with a decrease in the coverage. The phase diagram and the structure of two phases are illustrated in Fig. 7. According to our heat capacity measurements [18], the high-density solid undergoes an

order–disorder phase transition at 128 K accompanied by an excess entropy of approximately R ln 2 (Fig. 8), implying a reorientation of the molecules which was not discernible by diffraction techniques [19,20], mostly sensitive to the in-plane coordinates. In addition, an anomaly in the fluid phase is also found near the full coverage of the monolayer, which may indicate the presence of some ordered fluid like a liquid-crystalline phase.

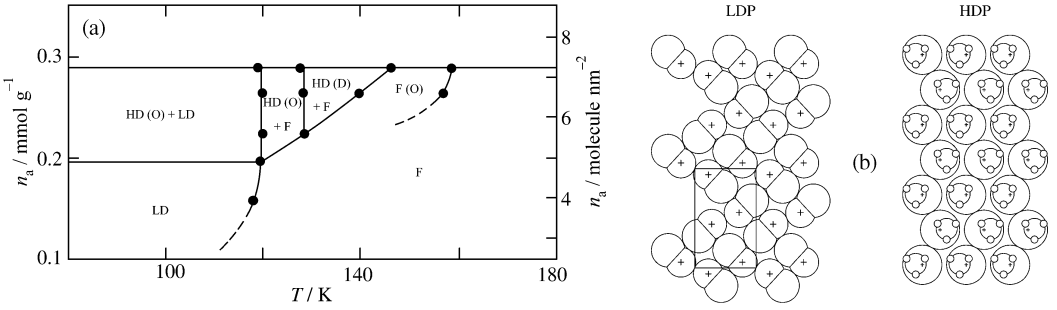

Fig. 7 (a) Phase diagram of CH_3Cl/graphite [18]. (b) Structure of CH_3Cl/graphite [19].

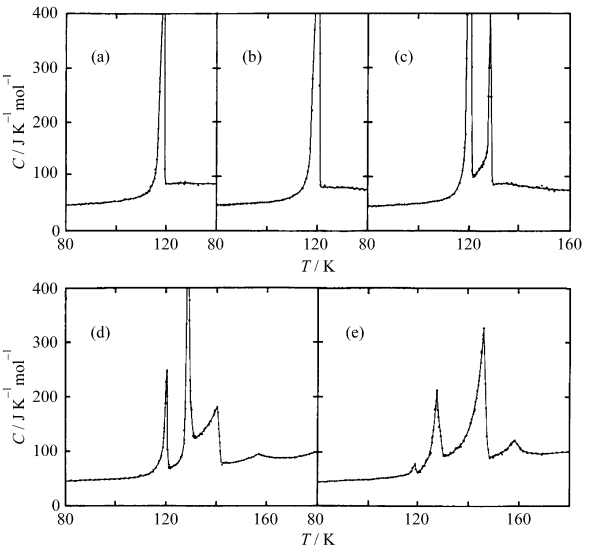

Fig. 8 Heat capacities of CH_3Cl/graphite [18]. The coverages are (a) 0.156, (b) 0.196, (c) 0.222, (d) 0.263, and (e) 0.288 mmol g^{-1}.

While the existence of the liquid–liquid transition was evidenced by a later diffraction experiment [21], the transition in the high-density solid phase was disbelieved by the same authors. However, the large entropy gain (R ln 2) must be explained somehow. Further investigation is needed by other methods.

ORIENTATIONALLY DISORDERED MONOLAYERS ON GRAPHITE

In the bulk, orientationally disordered crystals are characterized by a small entropy of melting (less than 20 J K^{-1} mol^{-1}) and the existence of a phase transition below which the crystal becomes brittle [22]. The large entropy change at the transition point suggests a considerable motional disorder in the disor-

dered phase. In fact, overall rotation of a molecule is highly excited, and even the self-diffusion is appreciable [23]. Tetramethyl compounds of the group-IV, $M(CH_3)_4$, where M = C, Si, Ge, Sn, or Pb, have been a favored subject for the study of the overall rotation of the molecule as well as the rotational dynamics of the CH_3 groups. Among those compound, however, neopentane (M = C) is the only crystal hitherto known to have an order–disorder phase transition [24]. The next compound of this series, tetramethylsilane (TMS) forms such disordered crystal only as a metastable (α) phase [25,26]. Two other phases (another metastable β and stable γ phases) are both ordered. In connection with those earlier studies for bulk solids, we investigated the adsorbed monolayers with the main point of the interest centered on whether those molecules could form the similar disordered phase. It was found that the monolayers of neopentane, TMS [27], and tetramethylgermane (M = Ge) [28] on graphite exhibit an order-disorder phase transition in the 2D solid, while those for M = Sn and Pb do not show such transition [29–31].

Heat capacity measurements showed that the neopentane monolayer exhibits a 2D solid–solid phase transition at 59 K (Fig. 9a). The mechanism of the phase transition is an orientational order–disorder type. In fact, incoherent neutron scattering revealed a beautiful quasielastic contribution in the high-temperature phase (Fig. 9b), indicating that the orientation of the whole molecule is disordered. It is interesting to note here that the 2D solid–solid phase transition is very sharp, being first-order, whereas the 2D melting is rather broad or continuous.

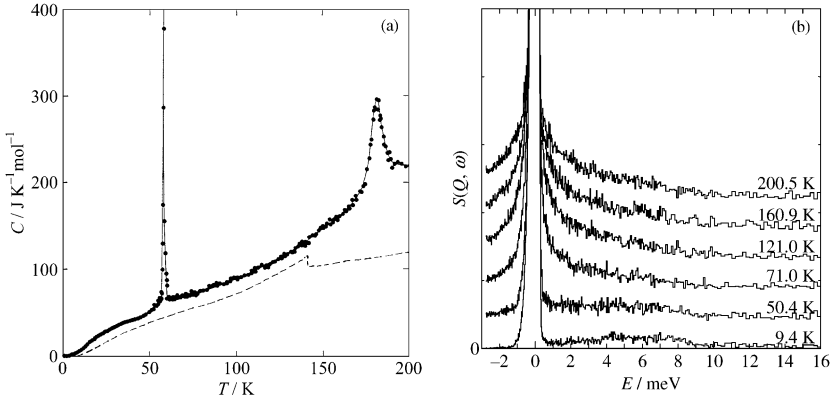

Fig. 9 (a) Heat capacity of the neopentane monolayer on graphite. (b) Quasielastic neutron scattering obtained for the neopentane monolayer on graphite.

For the monolayers of TMS/graphite, calorimetric investigation demonstrated two remarkable features [27]: (1) occurrence of an orientational order–disorder phase transition in the 2D solid (at 107 K at coverage $\theta < 1$ and at 138 K at $1 < \theta < 2$) accompanied by a large entropy change (ranging from R ln 8 to R ln 3) depending on the coverage, and (2) possible formation of a fluid bilayer around 220 K, above the 2D critical temperature. A high-resolution incoherent neutron-scattering experiment reveals a considerable motional disorder in the disordered 2D solid. The similar results are obtained also for TMS monolayers adsorbed on the MgO (100) surface [32,33].

ODD–EVEN VARIATION IN STRUCTURE OF ALKANE MONOLAYERS ON GRAPHITE

The structure of adsorbed monolayers of pure linear alkanes was studied by X-ray and neutron diffraction. They exhibit a pronounced odd–even alternation in structure with alkyl chain length, particularly for the shorter members of the series. As illustrated in Fig. 10, odd members have molecules that are essentially parallel to each other, belonging to 2D space group *cm* [34], which contrasts with the herringbone or zig-zag array of the even members, belonging to *pgg* [35]. These structures are most likely related to the partially commensurate nature of the adsorbed layers. In fact, the solid monolayers formed at the liquid–graphite interface (see in the next section) have structures fully commensurate with the underlying graphite for *n*-heptane ($9a_g \times \sqrt{3}a_g$), *n*-octane ($5\sqrt{3}a_g \times 2a_g$) and *n*-nonane ($11a_g \times \sqrt{3}a_g$), where a_g is the graphite lattice parameter, 0.2456 nm. *n*-Decane deviates slightly from the fully commensurate ($6\sqrt{3}a_g \times 2a_g$) lattice, being only uniaxially commensurate along the long (*a*) axis [34,35].

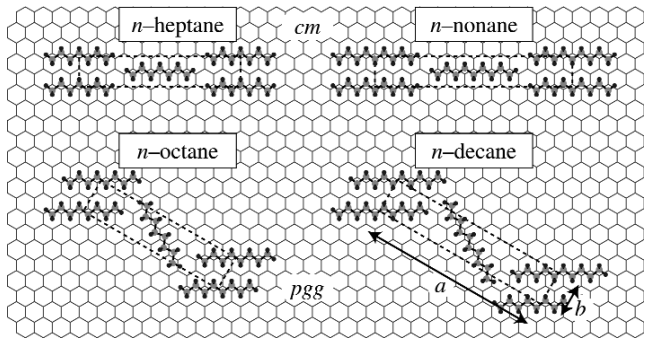

Fig. 10 Structure of the monolayers of *n*-heptane, *n*-octane, *n*-nonane, and *n*-decane [37].

Such odd–even alternation in symmetry is one of the key elements in understanding the mixing behavior of those compounds on the surface [36,37]. Binary mixtures of linear alkanes adsorbed on graphite are investigated by X-ray diffraction (Fig. 11) [37]. Monolayers of *n*-heptane and *n*-nonane, which belong to the same 2D space group, mix continuously over the whole range of composition. In contrast, *n*-nonane and *n*-decane belonging to different space groups have only limited miscibility. Interestingly, the isomorphous monolayers of *n*-octane and *n*-decane form a molecular compound, where no well-defined coherency exists along the *b*-axis.

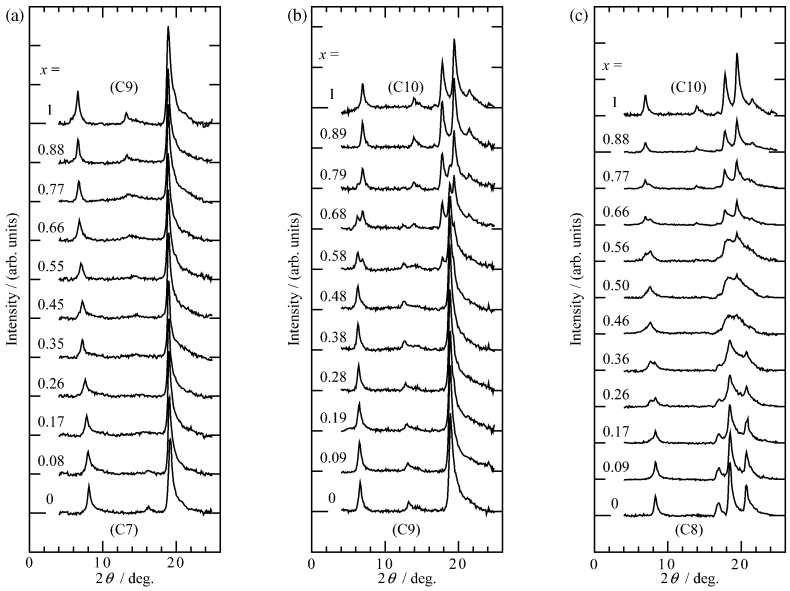

Fig. 11 Mixing behavior of the adsorbed monolayers on graphite for (a) *n*-heptane/*n*-nonane, (b) *n*-nonane/*n*-decane, and (c) *n*-octane/*n*-decane obtained by X-ray diffraction [37].

2D SOLIDS FORMED AT LIQUID–GRAPHITE INTERFACES

When we explored the multilayer coverages of alkanes, alkanols, and carboxylic acids adsorbed on graphite [38–51], we found that incoherent elastic neutron scattering is a powerful technique for the investigation of molecular layers adsorbed at buried solid–liquid interfaces. The idea is simple [38,39]: Neutrons scattered by static nuclei (located in solid) do not change energy on scattering, which is so-called elastic scattering. When the sample nuclei are moving (in liquid) then there is exchange of energy, which is so-called inelastic scattering. This simple idea provides a powerful tool to identify the amounts of solid- and liquid-like adsorbed material and their variations with temperature. This approach was used to identify the formation of solid monolayers that coexist with the bulk liquid as well as a solid surface. The strength of scattering varies from element to element and thus provides an ideal tool to investigate selectively the motions of a protonated adsorbate on a nonprotonated surface such as graphite [40], because the scattering is dominated by the strong incoherent contribution from the protonated adsorbate. An appropriate instrument, a high-resolution inelastic neutron spectrometer, is needed.

We found that in most cases a 2D solid monolayer is formed at the interface between the liquid and graphite. One of the examples for the incoherent neutron scattering is illustrated in Fig. 12a [41]. In most cases, the layers were found to melt approximately 10 % higher than the melting points of the bulk materials. The derived areas per molecule in the solid layers are consistent with the molecules lying with their long axis parallel to the surface [42]. Such monolayers have an important role in many interfacial phenomena such as detergency and lubrication. Calorimetry is useful to identify the melting point. An interesting odd–even alternation in the melting point of the monolayers is found for linear alcohols (Fig. 12b) [43].

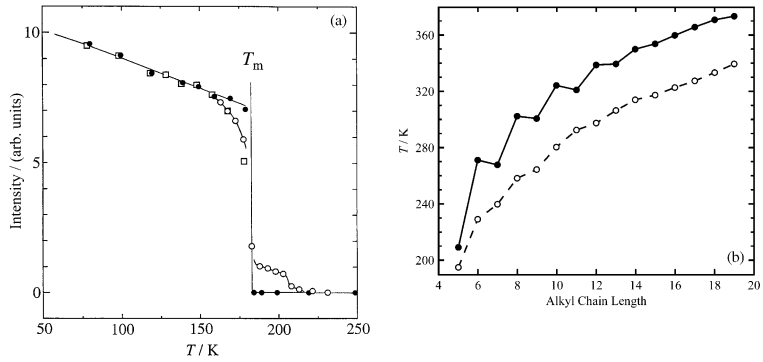

Fig. 12 (a) Incoherent elastic neutron scattering from 10 monolayers of *n*-heptane adsorbed on graphite (open marks) and the bulk *n*-heptane (filled marks) [41]. (b) Melting points of the bulk (open marks) and adsorbed monolayers (filled marks) of the primary alcohols [43].

The binary systems were also investigated [44–49], where the combination of calorimetry, incoherent elastic neutron scattering and neutron diffraction has been used to demonstrate the formation of solid layers and to characterize the adsorbed layer in some detail including the absolute composition and melting temperature as a function of solution composition. A typical mixing behavior is displayed in Fig. 13 for the system of alkanols [46,50]. Layer-by-layer surface freezing phenomenon was also observed in this system [51]. A 2D isomorphism coefficient is proposed to express how the unit cells must be quantitatively similar for two components to mix each other in the 2D solid [47,50].

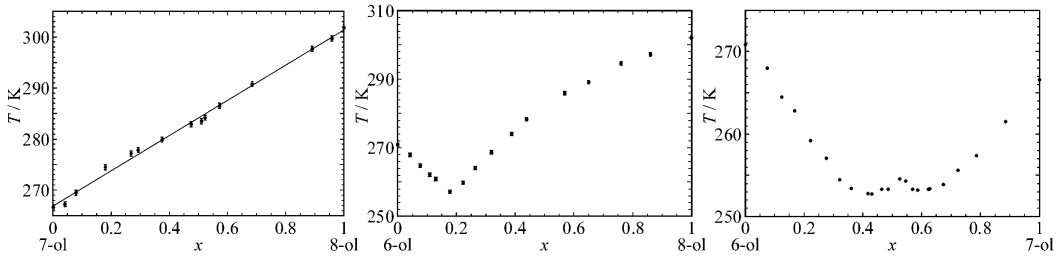

Fig. 13 Typical mixing behavior obtained for the alkanol monolayers formed at the liquid–graphite interface, showing complete miscibility (7-ol/8-ol), phase separation (6-ol/8-ol), and compound formation (6-ol/7-ol).

2D NATURE OF ICE FORMED IN CRYSTALLIZATION FROM THE SOLUTION

Rather recently, we found a 2D ice structure which appears in the initial stage of crystallization of aqueous solutions from the undercooled state [52]. Although the final crystal form of ice is the ordinary hexagonal I_h, the initial stages of nucleation from solution have been reported to show crystallites which appear more like the cubic phase of ice [53]. Here, neutron diffraction data from ice formed in glycerol solutions after quenched are presented.

Figure 14a shows the patterns obtained from 55 % (in mass) glycerol solution as a function of temperature. The pattern at 177 K is characteristic of a disordered (undercooled) water, suggesting that the system has been successfully quenched on the timescale of water and glycerol relaxation. The patterns remain essentially unchanged until 180 K when peaks begin to appear. All the patterns in Fig. 14a at higher temperatures essentially consist of three peaks with index as (100), (002), and (101) reflections of the ice I_h structure. The pattern at 190 K shows a particularly interesting form. Although the (002) reflection is well developed, the (100) reflection is weak and has a pronounced "saw-tooth" asym-

metry, characteristic of diffraction from 2D layers [54]. Significantly, the (101) reflection is essentially absent. These three characteristic features can be interpreted as follows: The appearance of a 2D peak-shape for the (100) reflection indicates the formation of layers of water molecules in the *ab* plane of the ice I_h structure. These layers are clearly crystalline with a significant extent (estimated at some 20 nm) or the peak would be far broader. The well-developed (002) reflection indicates that these layers are also stacked in the *c* direction in an ordered fashion with the bulk periodicity. However, there appears to be a serious miscorrelation between the different layers in the stacks such that the reflections of the type (H0L) are not formed. One can consider this to arise from the lack of orientational and/or positional order between the layers. Related layer disorder is at the origin of the differences between cubic and hexagonal ice. This simple disordered structure can account for all the peaks in the experimental patters simultaneously. However, we cannot exclude the possibility that we have different structure coexisting. For example, coexistence of both cubic ice and some 2D layers could also account for the experimental data. Either way, the observation of the peak characteristic of a 2D ice layer structure is unique. The disappearance of the 2D character of the (100) reflection and the growth of the (101) reflection are consistent with a reorientation and location of the different ice layers into the ordinary ice I_h structure.

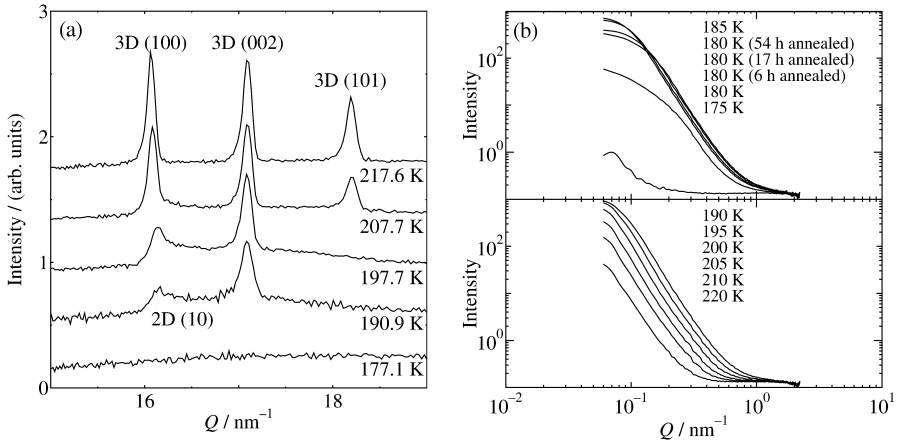

Fig. 14 (a) Neutron diffraction patterns from glycerol water (D_2O) mixture at 55 % (in mass) quenched to 78 K and then heated to the temperatures indicated. (b) Small-angle neutron scattering from the same solution.

Small-angle neutron scattering (Fig. 14b) demonstrates that at 180 K the crystallites of ice appear to develop their surface area significantly. As the ordinary ice grows, the size of the crystallites becomes larger to have the bulk ice. It should be mentioned here that such a novel form of ice is formed at low temperature from glycerol solutions. The role of glycerol, which is present in the solution studied, is expected to be important both in kinetic terms, as glycerol solutions are more viscous than pure water, and in stabilizing different ice faces by adsorption. Further study will be needed to characterize the kinetics of the crystallization and the driving forces for the initial formation of such a novel form of ice.

CONCLUSIONS

The synergetic use of X-ray diffraction, neutron scattering, and calorimetry to study the adsorbed layers has led to considerable progress in the understanding of the structure, dynamics, and thermodynamic behavior in detail, even at the level of a fraction of a monolayer and in multicomponent mixtures. It is obvious that no one technique, either experimental or theoretical, will provide sufficient information to describe such monolayers fully.

ACKNOWLEDGMENTS

I thank H. Chihara (Osaka), S. M. Clarke (Cambridge), T. Matsuo (Osaka), N. Sakisato (Osaka), and R. K. Thomas (Oxford) for their collaboration and participation in various aspects of this research. The late Prof. J. A. Morrison, who brought me to this world more than 20 years ago, is also acknowledged. This research was supported by JSPS, a Grant-in-Aid for Scientific Research (A) No. 16205001.

REFERENCES

1. For a review on physisorbed layers, see (a) J. G. Dash, J. Ruvalds (Eds.). *Phase Transitions in Surface Films*, Plenum, New York (1980); (b) H. Taub, G. Torzo, H. J. Lauter, S. C. Fain Jr. (Eds.). *Phase Transitions in Surface Films 2*, Plenum, New York (1991).
2. J. O. Clayton, W. F. Giauque. *J. Am. Chem. Soc*. **54**, 2610 (1932).
3. T. Atake, H. Suga, H. Chihara. *Chem. Lett.* 567 (1976).
4. K. Morishige, C. Mowforth, R. K. Thomas. *Surf. Sci.* **151**, 289 (1985).
5. A. Inaba, T. Shirakami, H. Chihara. *Chem. Phys. Lett.* **146**, 63 (1988).
6. A. Inaba, H. Chihara. *Can. J. Chem.* **66**, 703 (1988).
7. A. Inaba, T. Shirakami, H. Chihara. *J. Chem. Thermodyn.* **23**, 461 (1991).
8. K.-D. Kortmann, B. Leinböck, H. Wiechert, S. C. Fain, N. Stüßer. *Physica B* **234–236**, 167 (1997).
9. A. Inaba, T. Shirakami, H. Chihara. *Surf. Sci.* **242**, 202 (1991).
10. M. V. Smalley, A. Hüller, R. K. Thomas, J. W. White. *Mol. Phys.* **44**, 533 (1981).
11. A. Inaba, J. Skarbek, J. R. Lu, R. K. Thomas, C. J. Carlile, D. S. Sivia. *J. Chem. Phys.* **103**, 1627 (1995).
12. A. Inaba, S. Ikeda, J. Skarbek, R. K. Thomas, C. J. Carlile, D. S. Sivia. *Physica B* **213/214**, 643 (1995).
13. A. Inaba. *Physica B* **202**, 325 (1994).
14. K. Maki. *J. Chem. Phys.* **74**, 2049 (1981).
15. A. Inaba, J. A. Morrison. *Bull. Chem. Soc. Jpn.* **61**, 25 (1988).
16. P. C. Ball, A. Inaba, J. A. Morrison, M. V. Smalley, R. K. Thomas. *J. Chem. Phys.* **92**, 1372 (1990).
17. A. Inaba, H. Chihara, S. M. Clarke, R. K. Thomas. *Mol. Phys.* **72**, 109 (1991).
18. A. Inaba, H. Chihara. *J. Phys. Soc. Jpn.* **60**, 7 (1991).
19. K. Morishige, Y. Tajima, S. Kittaka, S. M. Clarke, R. K. Thomas. *Mol. Phys.* **72**, 395 (1991).
20. R. Nalezinski, A. M. Bradshaw, K. Knorr. *Surf. Sci.* **393**, 222 (1997).
21. S. Grieger, W. Press. *Europhys. Lett.* **33**, 193 (1996).
22. J. Timmermans. *J. Chim. Phys.* **35**, 331 (1938).
23. For a review on plastic crystals, see: J. N. Sherwood. *The Plastically Crystalline States. Orientationally Disordered Crystals*, John Wiley, New York (1979).
24. G. Aston, G. H. Messerly. *J. Am. Chem. Soc.* **58**, 2354 (1936).
25. M. Harada, T. Atake, H. Chihara. *J. Chem. Thermodyn.* **9**, 523 (1977).
26. T. Atake, H. Chihara. *Chem. Phys. Lett*. **56**, 330 (1978).
27. A. Inaba, N. Sakisato, T. Matsuo. *Chem. Phys. Lett.* **340**, 400 (2001).
28. W. A. Caliebe, J. Süßenbach, B. Asmussen, W. Press. *Surf. Sci.* **337**, 92 (1995).
29. H. Shechter, R. Brener, J. Suzanne, S. Bukshpan. *Phys. Rev. B* **26**, 5506 (1982).
30. M. Strzelczyk, N. Haack, B. Asmussen, J. Süßenbach, W. Press, J. Z. Larese. *Surf. Sci.* **376**, 339 (1997).
31. B. Asmussen, M. Strzelczyk, W. Press, J. Z. Larese. *Surf. Sci.* **406**, 138 (1998).
32. N. Sakisato, A. Inaba, T. Matsuo. *Appl. Phys. A* **74** (Suppl.), S1373 (2002).
33. N. Sakisato, A. Inaba, T. Matsuo. *J. Thermal Anal. Calorim.* **70**, 353 (2002).

34. T. Arnold, C. C. Dong, R. K. Thomas, M. A. Castro, A. Perdigon, S. M. Clarke, A. Inaba. *Phys. Chem. Chem. Phys.* **4**, 3430 (2002).
35. T. Arnold, R. K. Thomas, M. A. Castro, S. M. Clarke, L. Messe, A. Inaba. *Phys. Chem. Chem. Phys.* **4**, 345 (2002).
36. M. A. Castro, S. M. Clarke, A. Inaba, R. K. Thomas, T. Arnold. *Phys. Chem. Chem. Phys.* **3**, 3774 (2001).
37. A. Inaba, S. M. Clarke, T. Arnold, R. K. Thomas. *Chem. Phys. Lett.* **352**, 57 (2002).
38. M. A. Castro, S. M. Clarke, A. Inaba, R. K. Thomas. *J. Phys. Chem. B* **101**, 8878 (1997).
39. M. A. Castro, S. M. Clarke, A. Inaba, R. K. Thomas. *Physica B* **241–243**, 1086 (1998).
40. M. A. Castro, S. M. Clarke, A. Inaba, C. C. Dong, R. K. Thomas. *J. Phys. Chem. B* **102**, 777 (1998).
41. M. A. Castro, S. M. Clarke, A. Inaba, T. Arnold, R. K. Thomas. *J. Phys. Chem. Solids* **60**, 1495 (1999).
42. M. A. Castro, S. M. Clarke, A. Inaba, T. Arnold, R. K. Thomas. *J. Phys. Chem. B* **102**, 10528 (1998).
43. S. M. Clarke, L. Messe, C. Whitehead, A. Inaba, R. K. Thomas, T. Arnold. *Appl. Phys. A* **74** (Suppl.), S1072 (2002).
44. M. A. Castro, S. M. Clarke, A. Inaba, T. Arnold, R. K. Thomas. *Phys. Chem. Chem. Phys.* **1**, 5017 (1999).
45. M. A. Castro, S. M. Clarke, A. Inaba, R. K. Thomas, T. Arnold. *J. Phys. Chem. B* **105**, 8577 (2001).
46. L. Messe, S. M. Clarke, C. C. Dong, R. K. Thomas, A. Inaba, M. D. Alba, M. A. Castro. *Langmuir* **18**, 9429 (2002).
47. S. M. Clarke, L. Messe, J. Adams, A. Inaba, T. Arnold, R. K. Thomas. *Chem. Phys. Lett.* **373**, 480 (2003).
48. A. K. Bickerstaffe, L. Messe, S. M. Clarke, J. Parker, A. Perdigon, N. P. Cheah, A. Inaba. *Phys. Chem. Chem. Phys.* **6**, 3545 (2004).
49. L. Messe, A. Perdigon, S. M. Clarke, A. Inaba, T. Arnold. *Langmuir* **21**, 5085 (2005).
50. L. Messe, S. M. Clarke, T. Arnold, C. C. Dong, R. K. Thomas, A. Inaba. *Langmuir* **18**, 4010 (2002).
51. L. Messe, A. Perdigon, S. M. Clarke, M. A. Castro, A. Inaba. *J. Colloid Interface Sci.* **266**, 19 (2003).
52. A. Inaba, N. Sakisato, A. K. Bickerstaffe, S. M. Clarke. *J. Neutron Res.* **13**, 87 (2005).
53. D. C. Steytler, J. C. Dore, C. J. Wright. *J. Phys. Chem.* **87**, 2458 (1983).
54. B. E. Warren. *Phys. Rev*. **59**, 693 (1941).

Contribution No. 98 from the Research Center for Molecular Thermodynamics.